Measurements and Predictions of Light Scattering by Clear Coatings

Mary E. McKnight, Theodore V. Vorburger, Egon Marx, Maria E. Nadal, P. Yvonne Barnes, and Michael A. Galler
National Institute of Standards and Technology
Gaithersburg, MD 20899

To be published in Applied Optics -- May 2001

Comparisons are made between calculated and measured angle-resolved light scattering distributions from clear dielectric isotropic epoxy coatings over a range of root-mean-square (rms) roughness conditions, resulting in strongly specular scattering to diffuse scattering characteristics. Calculated distributions are derived from topography measurements performed with interferometric microscopes. Two methods of calculations are used. One determines the intensity of scattered light waves using a phase integral in the Kirchhoff approximation. The other is based on the reflection of light rays by locally flat surfaces. The angle-resolved scattering distributions for the coatings are measured using the spectral tri-function automated reference reflectometer (STARR) developed by the National Institute of Standards and Technology. Comparisons between measured and calculated results are shown for three surfaces with rms roughness values of approximately 3 nm, 150 nm and 800 nm for an angle of incidence of 20°.

1. Introduction

Appearance is a critical performance parameter for most industries, including automotive, textile, paper, and plastic. For example, the color and appearance of automobiles is reported to be the major influence in about half of car purchases.[1] The visibility of warning signs and camouflaged objects also depends on the optical properties of the materials. Furthermore, continuing demands for new materials and manufacturing processes, as well as the customer expectations for improved appearance quality, create a need for advanced appearance measurements and models.

This study is part of an appearance project[2] at the National Institute of Standards and Technology (NIST) whose purpose is to develop advanced methods for appearance characterization and predictive image rendering of surfaces through a systems approach using optical metrology, descriptions of surface and subsurface microstructure, mathematical modeling, and computer rendering. The first step of the project is to relate the optical properties of the raw materials to the microstructure of the manufactured material. The next steps are to characterize the microstructure, to measure the optical reflectance properties of the manufactured materials, and to mathematically model the optical reflectance properties based on the microstructure. Finally, scientifically accurate rendering models are used to create images of objects with the measured or modeled reflectance values. In this way, relationships between material properties and optical reflectance can be developed and used to predict the appearance of materials.

The first samples chosen to demonstrate the approach consisted of clear dielectric epoxy coatings on a black glass substrate. Surface scattering is dominant in these samples. Pigmented coatings in which both bulk and surface scattering are important are being used in the next phase of the project. The clear coating samples were fabricated to test the model over a range of root-mean-square (rms) roughness conditions, resulting in strongly specular scattering to diffuse scattering characteristics. The angle-resolved

light scattering measurements were performed using the NIST spectral tri-function automated reference reflectometer (STARR).[3] The topographical data used in the optical scattering models were determined using interferometric microscopy. Two methods were used to calculate angle-resolved light scattering for comparison with the corresponding measured values. One method determined the intensity of scattered light waves using a phase integral in the Kirchhoff approximation.[4] The other method was based on the reflection of light rays by locally flat surfaces (see, for example, Ref. 5). Bendler *et al*.[6] carried out a comparable experiment in which they calculated an absolute scattering distribution for light waves for a perfectly conducting surface using a statistical model of the surface. This study is different in that the dielectric sample surfaces transmit light in addition to scattering light and a topographical map of the surface is used to calculate the scattered light.

The study described in this paper serves as a test of three independent procedures: the surface measurements, the optical scattering measurements, and the optical scattering calculations. Assuming that the two types of measurements are accurate, then agreement between the calculated results and the scattering measurements serves as a demonstration of the validity of different approximations used in reflectance theory. The agreement also validates calculations done in the ray approximation, which were used in a demonstration of computer rendering based on the reflectance of these surfaces.[7]

The simulation of the measured intensities by the phase integral involves a number of constant factors that are difficult to determine, including one that takes into account the refraction at the dielectric surface. The ray counting method does not provide an absolute intensity either. Thus angular distributions of measured and computed light intensities that have been normalized to 1 in the specular direction were compared.

2. Experimental

A. Sample Preparation

The samples for this study were made of a clear 100 % solid amine-cured epoxy coating on a black glass substrate. Samples were prepared, as illustrated in Fig. 1, by casting the coating against 50 mm by 50 mm molds of varying roughness. Black glass (Schott Glass,[8] NG-1, 3 mm thickness) was used as the mold to prepare the sample having the smoothest surface. The remaining molds were prepared using a matte finished, steel panel (rms roughness of ~1 μm) as the base material. The roughness of the base material was modified by spin coating with a solution containing a surface-modifying polymer. Polymer solutions having volume solid fractions increasing from 10% to 45 % were used to systematically prepare molds having decreasing rms roughness values from about 800 nm to 100 nm, as estimated from mechanical (stylus) profiling data.[9] The roughness molds decreased with increasing concentration of the polymeric solution, as predicted.[10]

Sets of epoxy-coating samples were prepared by treating each mold with a release agent, constructing sides ~1.3 mm thick using a rubber gasket material, and clamping a black-glass substrate material against the mold using spring-loaded clamps (see Fig. 1). The assembly was held upright and the premixed, degassed epoxy coating was introduced through a hole in a bottom corner of the glass. A hole in the opposite corner of the glass substrate served as a vent. By forcing epoxy into the lower hole, trapped air bubbles in the coating were minimized. Next, the epoxy was heat-cured according to the epoxy-manufacturer's instructions and then the whole was disassembled. The actual size of the cured-coating sample was about 35 mm by 35 mm, smaller than the black glass substrate due to the gasket and the holes drilled in the substrate.

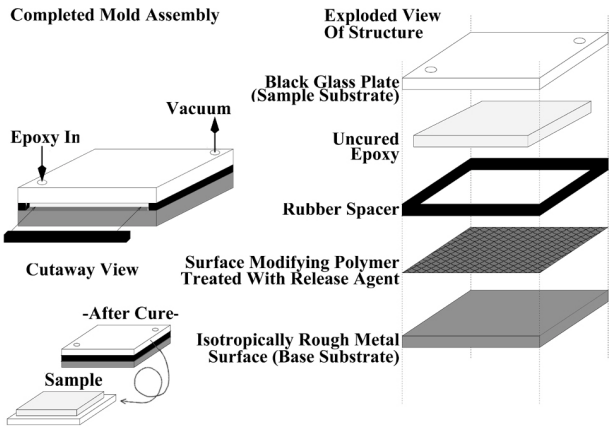

Figure 1. Schematic diagram illustrating fabrication of clear-epoxy samples with controlled roughness.

Except for the sample cast against black glass, estimates of the roughness of representative samples were obtained from profile measurements using a stylus-profiling instrument. Samples taken from the sets corresponding to stylus roughnesses of 640 nm (Sample A) and 115 nm (Sample b) and the black glass replicate (Sample C) were selected for the study.

The index of refraction of the black substrate glass and the epoxy coating are 1.52 and 1.55 at a wavelength of 587.6 nm, respectively. The estimated expanded uncertainty of the index of refraction values is less than 0.01. Because of the slight difference in the refractive indices of the epoxy and the glass, the intensity of the light reflected from the glass/coating interface is small compared to that of the light scattered from the surface (~0.01 % for an angle of 20 ° and ~0.1 % for an angle of 60 °, estimated using the Fresnel equations).

B. Optical Scattering Measurements

Angle-resolved scattering from rough surfaces is often described using the bidirectional reflectance distribution function (BRDF), which is the ratio of the differential radiance to the differential irradiance.[11] Irradiance is the light flux or power incident per unit area while radiance is the light flux scattered from the sample, in a given direction, per unit projected area of the sample viewed from that direction, per unit solid angle. For the case of a nearly collimated incident beam,

$$\mathrm{BRDF} \approx \frac{P_s / (\Omega_s \cos\theta_s)}{P_i}, \tag{1}$$

where the indices *i* and *s* stand for incident and scattered quantities, respectively, P is flux or power, Ω is the solid angle, and θ is the polar angle. Reflectance ρ is defined as the ratio of the powers,

$$\rho = P_s / P_i = \mathrm{BRDF} \cdot \Omega_s \cos\theta_s \quad . \tag{2}$$

Absolute measurements of in-plane bidirectional scattering were performed using STARR[3,12] at NIST. Figure 2 is a schematic of the instrument. The incident radiant flux is a collimated, monochromatic, polarized beam with a diameter of 14 mm and bandwidth of 10 nm. For bidirectional measurements, a lens focuses either the collimated incident beam or the image of the front of the sample onto the detector, a silicon photodiode. The sample is positioned either in or out of the incident beam path using two

orthogonal translational stages. Two rotation stages determine the angle of incidence of the beam on the sample and the viewing angle of the photodiode. The detector assembly rotates around the sample holder at a constant distance of 672.6 mm, measured from the sample rotation axis to the 31.8 mm diameter aperture stop in the detector. Therefore the detector aperture subtends an angle of approximately 2.7°.

The reflectance is calculated from measurements of the incident and reflected radiant fluxes. The incident flux is measured with the sample positioned out of the beam path and the receiver positioned to accept the incident beam. The reflected radiant flux is measured with the sample positioned in the beam path with the sample and the detector positioned to measure the reflected flux at the desired geometry.

The angular convention is shown in Fig. 3. The angle of incidence θ_i and scattering angle θ_s are measured from the normal to the sample. In this convention, the specular direction for an angle of incidence θ_i is along $-\theta_i$.

The reflectance of the each of the three clear-epoxy coating samples and a highly polished black glass sample were measured at wavelengths of 500 nm, 550 nm, and 600 nm for angle of incidences of 20º, 45º, 60º, and 70° and viewing angles from −75º to 75º in steps of 1º. Results are shown only for 550 nm and, with exception of some measured data of the absolute reflectance, for 20° because not much additional information is gained from the comparison of calculated and measured relative reflectances for these samples at other wavelengths and angles.

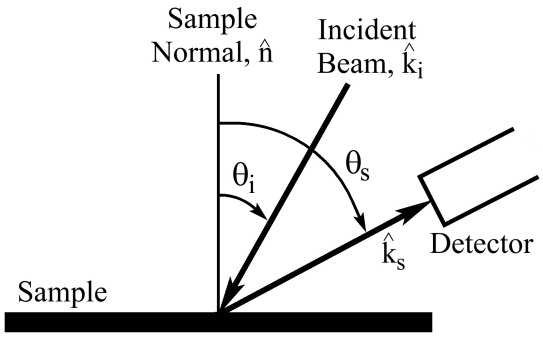

Figure 2. Schematic diagram of STARR with all the major components labeled in (a). Part (a) depicts the incident-flux measurement and (b) depicts the reflected-flux measurement.

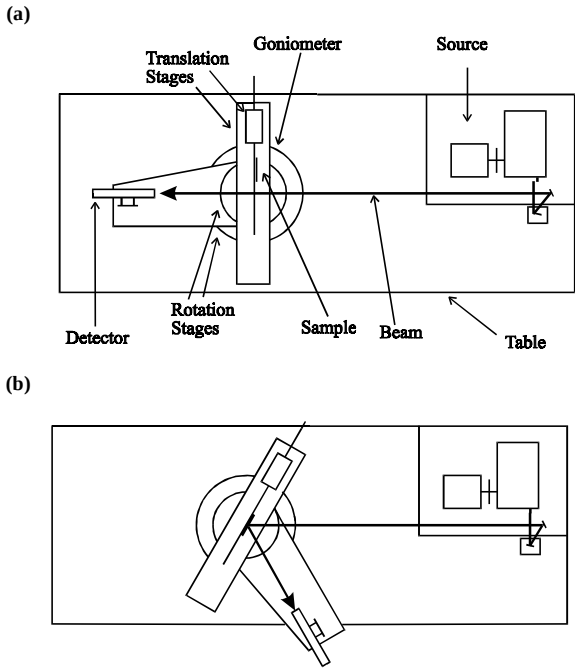

Figure 3. Convention for incidence and scattering angles.

C. Surface Topography Measurements

The surface topographies of the three clear-epoxy coating samples were measured by interferometric microscopy to provide input for the optical scattering calculations. The topography data z are described by a function $\zeta(x,y)$, where ζ represents the height of the surface at a lateral position (x,y). This is a digital representation in which the x,y positions are linked to pixel elements in the camera of the microscope, which are equally spaced in x and in y. Therefore, the point (x,y) can be represented by $(i\Delta x, j\Delta y)$ where i and j are the pixel indices and Δx and Δy are the sampling intervals.

The surfaces of the samples were measured by the technique of scanning white light interferometric (SWLI) microscopy.[13,14] A typical SWLI microscope is shown in Fig. 4.[15] A wide band source of light is collimated and then focused through a beamsplitter in a cone of angles around normal incidence. Part of the light proceeds to the sample surface and part is reflected to the reference surface. The beams reflected by the sample and the reference are recombined and produce optimally-strong interference fringes on the camera when the optical path difference between them is zero. The topographic data are recorded as follows. The reference mirror is scanned vertically and the equal path condition is found for each pixel in the camera. The z positions for the equal path condition are a function of the sample surface topography. The z-position data for each pixel (x,y) yields the topographic map $\zeta(x,y)$.

Two different interferometric microscopes,[8,16,17] located at their respective manufacturer's sites, were used to measure the topographies of Samples A and B. The instrument parameters were slightly different for the two microscopes.

Table shows the nominal measurement parameters for the two microscopes. For both sets of topography measurements, the area of the sample measured by the STARR was positioned by eye under the microscope and an unblemished area was chosen for the measurement. No attempt was made to relocate th

measured area from one microscope to the other. Sample C was measured subsequently to A and B and was significantly smoother. Its surface topography was measured in three areas using a third microscope of the same type as Microscope 1 but in the phase shifting interferometry (PSI) mode,[18] rather than the SWLI mode. The PSI mode was used because the rms roughness of Sample C is approximately at the limit of vertical resolution of SWLI for this microscope, whereas PSI has subnanometer vertical resolution. The PSI technique is similar to SWLI microscopy and has essentially the same schematic diagram. Like SWLI microscopy, the surface topography is measured by continuously measuring the changes in the interferometric fringes over the surface as the reference surface is slowly scanned. However, monochromatic light is used and the surface topography is calculated with a different algorithm than that for SWLI.[19] Table I shows the measurement parameters.

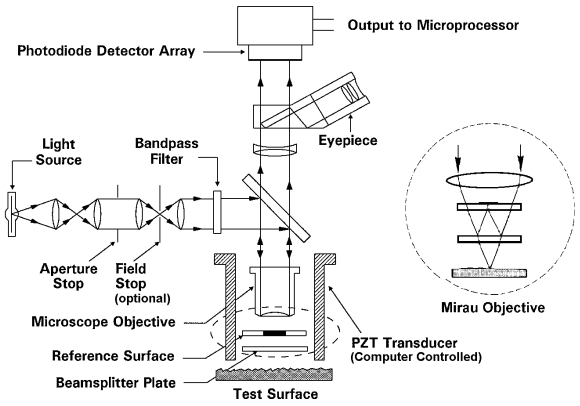

Figure 4. Schematic diagram of a typical interferometric microscope, which may be used either in the phase shifting mode or the scanning white light mode.

Table 1. Measurement Parameters for Scanning White-Light Interferometric Microscopes

Parameter	**SWLI Microscope 1[16]**	**SWLI Microscope 2[17]**	**PSI Microscope 3, Same type as 1**
Interferometer Configuration	Mirau	Mirau	Mirau
Nominal Pixel Spacing Δx, Δy	0.796 μm, 0.927 μm	2.25 μm, 2.25 μm	0.409 μm, 0.477 μm
Number of Pixels N_x, N_y	736, 480	320, 240	736, 480
Size of Measured Area $N_x\Delta x \times N_y\Delta y$	586 μm × 445 μm	720 μm × 540 μm	301 μm × 229 μm
Numerical Aperture	0.3	0.3	0.3
Number of Measured Areas	1	1	3
Samples Measured	A and B	A and B	C

3. Light Scattering Calculations

The intensity of light scattered by a rough surface specified by surface maps was calculated using two different methods. One method is based on the phase integral for the scattered field amplitude in the Kirchhoff approximation as derived by Beckmann.[4] The second method is based on the specular reflection of light rays by locally flat surfaces. Results were compared with intensities measured using STARR.

For the scattering calculations, the surface is represented by a topographic map as described in Subsection II.C. Light of wavelength λ is assumed to be incident along a direction given by the polar angle θ_i and the azimuthal angle ϕ_i. The derivation of the scattered light intensity assumes that the surface is perfectly conducting, although Beckmann extends the approach to finitely conducting media, such as dielectrics.[4]

In the phase integral approximation, the amplitude of the light scattered by a perfectly conducting rough surface in the direction given by the spherical coordinate angles θ_s and ϕ_s from an incident, monochromatic, electromagnetic plane wave is given by

$$\psi(\theta_i,\phi_i;\theta_s,\phi_s) = [F_3(\theta_i,\phi_i;\theta_s,\phi_s)/A]\int_\Sigma \exp\left[(i\vec{v}(\theta_i,\phi_i;\theta_s,\phi_s)\cdot\vec{r}(x,y)\right]dxdy, \tag{3}$$

where Σ is the projection of the illuminated region on the *xy*-plane and A its area,

$$F_3(\theta_i,\phi_i;\theta_s,\phi_s) = \frac{1+\cos\theta_i\cos\theta_s+\sin\theta_i\sin\theta_s\cos(\phi_i-\phi_s)}{\cos\theta_i(\cos\theta_i+\cos\theta_s)}, \tag{4}$$

$$\begin{aligned}\vec{v} = -k[&(\sin\theta_i\cos\phi_i+\sin\theta_s\cos\phi_s)\hat{e}_x+(\sin\theta_i\sin\phi_i+\sin\theta_s\sin\phi_s)\hat{e}_y\\ &+(\cos\theta_i+\cos\theta_s)\hat{e}_z],\end{aligned} \tag{5}$$

and $k = 2\pi/\lambda$. The amplitude has been normalized to that reflected by a flat surface.[4] It follows that

$$\begin{aligned}\vec{v}\cdot\vec{r} = -k[&(\sin\theta_i\cos\phi_i+\sin\theta_s\cos\phi_s)x+(\sin\theta_i\sin\phi_i+\sin\theta_s\sin\phi_s)y\\ &+(\cos\theta_i+\cos\theta_s)\zeta(x,y)].\end{aligned} \tag{6}$$

Note that the measured three dimensional topography is used for the calculation with no assumption of surface isotropy and that these equations reduce to those in Ref. 4 if we set $\phi_i = \pi$. The integral in Eq. (3) is approximated by a sum and a good approximation requires the use of at least ten points per wavelength. However, it is not possible to obtain data at such close intervals with an optical instrument. Therefore, a two-dimensional cubic spline was used to interpolate the topographical data on the surface. The interpolated points are chosen not to be equispaced to avoid possible problems with scattering by a (numerical) grating. Although STARR has the capability for measurements slightly outside the plane of incidence, for these experiments the detector was scanned only through the plane of incidence. Therefore, $\phi_s = \phi_i$ is used in all calculations to simulate this approach. The range of θ_s is extended to negative values by mapping $(\theta_S,\phi_S) \rightarrow (-\theta_S,\phi_S-\pi)$ for $\phi_s \geq \pi$.

If the illuminated surface is assumed to be a perfectly flat rectangle of sides L_1 and L_2, Eq. (3) reduces to

$$\psi(\theta_i,\phi_i;\theta_s,\phi_s) = F_3(\theta_i,\phi_i;\theta_s,\phi_s)\,\mathrm{sinc}(v_x L_1/2)\,\mathrm{sinc}(v_y L_2/2), \tag{7}$$

where v_x and v_y are given in Eq. (5). The sinc functions decrease rather slowly with increasing argument, which causes the computed scattered intensity to remain relatively large away from the specular direction, contrary to what happens experimentally. Because an actual light beam does not have a uniform intensity that suddenly drops to zero outside the patch, a beam profile was simulated using a windowing function, W(x,y). Then, Eq. (3) becomes

$$\psi(\theta_i,\phi_i;\theta_s,\phi_s) = [F_3(\theta_i,\phi_i;\theta_s,\phi_s)/A]\int_\Sigma W(x,y)[\exp(i\vec{v}(\theta_i,\phi_i;\theta_s,\phi_s)\cdot\vec{r}(x,y)]dxdy. \tag{8}$$

For a rectangular patch, it is assumed that $W(x,y) = W_1(x)W_2(y)$. Through investigations of a number of windows in calculations of light scattered by a sinusoidal surface,[20,21] it was concluded that the test function used by Schwartz in the theory of distributions gives the best computed results. This windowing function is

$$W(x) = \begin{cases} \exp\{\alpha[1-L_i^2/(L_i^2-x^2)]\}, & |x| \le L_i, \\ 0, & \text{elsewhere}, \end{cases} \tag{9}$$

for i = 1, 2. The value $\alpha = 0.1$ was used in calculations. The windowing function does not have to reflect the actual cross section of the incident beam of light, which covers a much larger region of the sample than the surface map. It is used here to avoid the numerical problems associated with a discontinuity at the edges of the surface map. The light beam is often assumed to have a Gaussian cross section, but calculations indicate that a Gaussian that remains close to 1 over a sizable fraction of the region of integration will have a jump at the edges that reproduces the problems associated with the rectangular window.[20,21]

An actual detector collects light over a solid angle. To compare with measured values of the scattered light intensity, the computed values can be integrated over the surface of the detector or they can be convolved with the measured instrument signature. The first approach requires computing the scattered intensity for a large number of angles, especially when the detector is positioned in the specular direction. The second approach is easier to implement and has been used in the calculations described here. The simulated intensity, $\bar{I}(\theta)$, is expressed as the integral of the product of the computed intensity, $I(\theta) = |\psi(\theta)|^2$, and the displaced signature of the instrument or response curve, $I_r(\theta)$, which is given by the unnormalized intensities measured by STARR in the absence of the sample. The simulated intensity then is

$$\bar{I}(\theta) = \int_{-\frac{1}{2}\pi}^{\frac{1}{2}\pi} I(\theta')I_r(\theta'-\theta)d\theta'. \tag{10}$$

This integration is carried out numerically. The function I(θ) varies rapidly near the specular direction, which means that the interval $\Delta\theta'$ has to be much smaller in that region than elsewhere. The number of points needed for the integration was determined by subdividing the original interval and analyzing the change in the result. If the change was larger than a preset fraction, the interval was again subdivided.

Because this model does not take into account the dielectric constant of the epoxy layer, the intensity of the scattered light can be computed only up to an overall factor. Thus, the measured and calculated intensities were compared by normalizing the curves to 1 in the specular direction.

The ray method used to determine the angular distribution of the scattered light is based on the assumption that an incident ray is reflected specularly by the surface, assumed to be locally approximated by a tangent plane.[5,22] The direction of the normal, $\hat{n}$, to the surface at a particular point is determined either by performing a least-squares fit of the distances from the neighboring points to a (tangent) plane through the given point or by fitting a cubic spline to the surface. The method used to compute the normal to the surface had a negligible effect on the resulting intensities. The execution time required to compute an intensity distribution using the ray method is much smaller than the time required to compute phase integrals. Consequently, this method can more easily be used to compute the BRDF for the purpose of

computer rendering, requiring intensities for many directions of incidence and scattering.[7] Computations based on the Kirchhoff approximation can be used to validate those using the ray approximation.

If $\hat{k}_i$ is in the direction of the incident wave, the direction, $\hat{k}''$, of the locally reflected wave is

$$\hat{k}'' = \hat{k}_i - 2\left(\hat{k}_i \cdot \hat{n}\right)\hat{n}\,. \tag{11}$$

If the axis of the j[th] detector position is along the direction of $\hat{r}_j$, the angle Δ between this axis and the local specular beam is given by

$$\cos\Delta = \hat{k}'' \cdot \hat{r}_j = \sin\theta'' \sin\theta_j \cos(\phi'' - \phi_j) + \cos\theta'' \cos\theta_j\,, \tag{12}$$

where θ'' and ϕ'' are the polar coordinates of $\hat{k}''$.

If the computed angle Δ is smaller than the half-aperture of the instrument, the reflected ray falls within the detector and the count for that detector is incremented by one unit. The approximation to the scattered intensity will then be proportional to the number of counts for the detector. Again the intensity distribution is normalized to 1 in the specular direction. The agreement of intensities obtained in this simple ray optics model with measured results and those obtained from the phase integral shows that a more elaborate ray intensity formula related to the surface curvature obtained in the geometric optics approximation is not needed.

A third method that can be used to compute the scattered light is a numerical solution of the exact integral equation that is equivalent to Maxwell's equations.[23] To simplify the problem, one can assume that a monochromatic plane wave is incident on a rough measured patch embedded in a flat surface of a dielectric half-space. The patch has to be tapered off into the plane. However, the memory requirements are such that only a small subset of the measured surface image can be used in the calculation. Thus, calculations using this method were not done. Another commonly used method is the first order vector theory.[24] However, this approximation is only valid if the rms roughness is much less than λ, a requirement that is not true for Samples A and B.

4. Results

A. Optical Scattering Measurements

Selected results of the optical scattering measurements are shown in Figs. 5 and 6, where a linear scale is used for the reflectance. Figure 5 shows the reflectance as a function of scattering angle for a 60° angle of incidence at 550 nm for all the samples and for black glass. The gonio-distribution of the reflectance is nearly symmetric about the specular angle, -60°. The light around the specular direction decreases as the surface roughness increases and more diffuse reflection is observed. The refractive index of the clear epoxy is ~2% larger than that of black glass, resulting in about a 7% increase in specular reflectance, consistent with the measured values shown in Fig. 5.

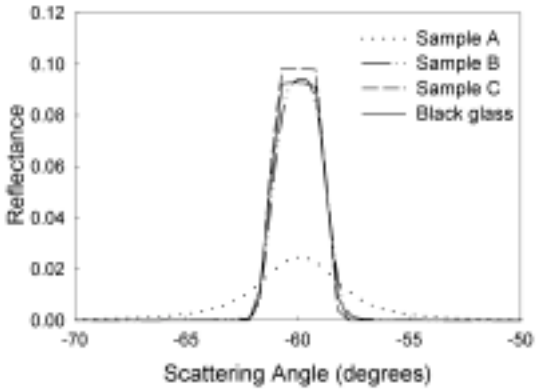

Figure 5. Measured reflectance as a function of observation (scattering) angle for Samples A, B, and C, and for a highly polished black glass specimen at 550 nm and 60° angle of incidence.

Figure 6 shows the absolute reflectance for Sample B for angles of incidence of 20°, 45°, and 60°. The samples appear more glossy as the angle of incidence increases from 20° to 60°, as predicted by the Fresnel equations, but the shapes of the curves near the specular direction do not depend strongly on the angle.

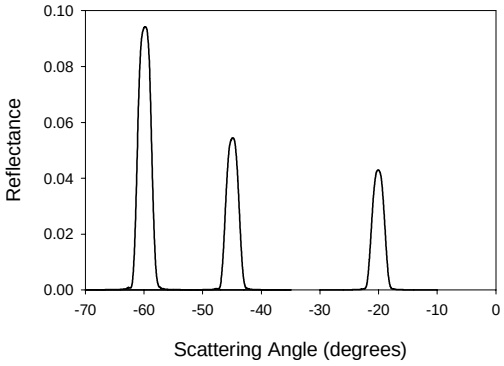

Figure 6. Measured reflectance of Sample B as a function of observation angle for incident angles of 20º, 45º, and 60º.

The isotropy of the samples was investigated by measuring the absolute specular reflectance as the sample was rotated about the normal of the surface. Since the measured reflectances remain essentially constant, the epoxy layer is assumed to be isotropic over the 14 mm diameter illuminated region for the lateral scale relevant to this measurement.

Uncertainties were calculated according to the procedures outlined in Ref. 25. The type A uncertainty components, which are calculated by statistical methods, include source stability and detector noise and result in a relative uncertainty of 0.05%. Type B sources of uncertainty include wavelength, incident and viewing angles, and uniformity of the sample. The relative uncertainty due to the type B sources is 0.2%. The expanded uncertainty in the measured reflectance with a coverage factor k = 2 is 0.4% at 550 nm.

B. Surface Topography Measurements

Topography maps of the samples are shown in Figs. 7-11. The roughness scale as shown in the vertical bar in each figure was allowed to vary in order to display features in each image clearly. The measured rms roughnesses for the surface of Sample A were 805 nm and 871 nm, and for the surface of Sample B were 201 nm and 124 nm for SWLI Microscopes 1 and 2, respectively. The difference in rms roughness values suggest that the surfaces vary significantly on the measured lateral scale of ~0.5 mm. In addition, scratch-like marks were observed in Sample B in the area examined using SWLI Microscope 1 but not in the area examined using Microscope 2.

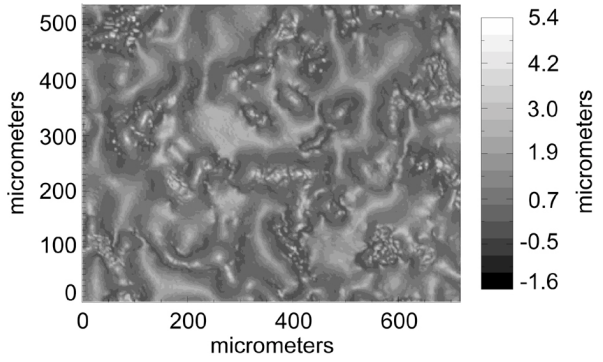

Figure 7. Surface topography map of Sample A as measured by SWLI Microscope 1; rms roughness = 805 nm.

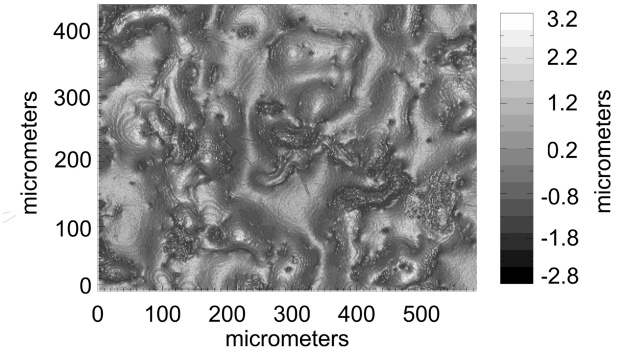

Figure 8. Surface topography map of Sample A as measured by SWLI Microscope 2; rms roughness = 871 nm.

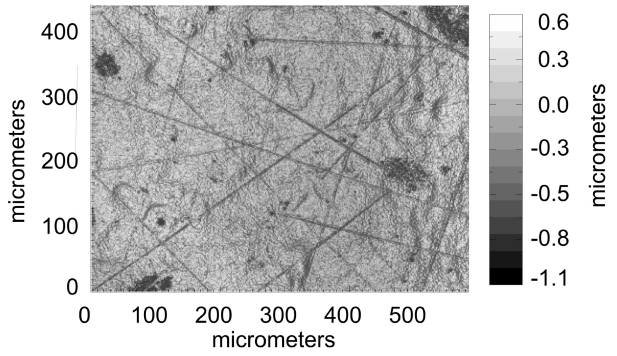

Figure 9. Surface topography map of Sample B as measured by SWLI Microscope 1; rms roughness = 201 nm.

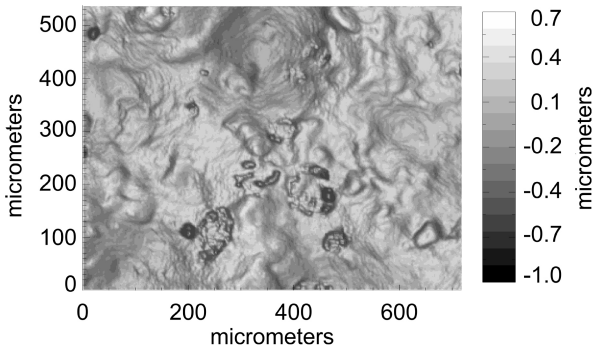

Figure 10. Surface topography map of Sample B as measured by SWLI Microscope 2; rms roughness = 124 nm.

The rms roughness values measured with the microscopes are larger than those measured with the stylus profiling instrument. The difference could be associated with the differences in the bandwidths of the two techniques. The bandwidth of spatial wavelengths in the topography maps extends from the optical resolution of the microscope, ~1 μm, to the size of the map itself, about 585 μm or 720 μm, larger than the bandwidth of the stylus measurements (250 μm).

Sample C was measured subsequently. Three areas were measured on this surface, all within the 14 mm wide area covered by the light scattering technique. The measured rms roughnesses of the three measured areas were 5.0 nm, 3.0 nm, and 2.2 nm. The topography map for the area with rms roughness of 5.0 nm is shown in Fig. 11. The variation of these measurements is again due to the nonuniformity of the specimen surface. The standard deviation of the three rms roughness measurements is 1.4 nm, ~41 % of the average value of 3.25 nm. The uncertainties arising from the instrument are considerably smaller than this. Notably, in PSI mode, the instrument is calibrated directly against the wavelength of light with a small obliquity correction factor required at the 20x magnification used in this study.

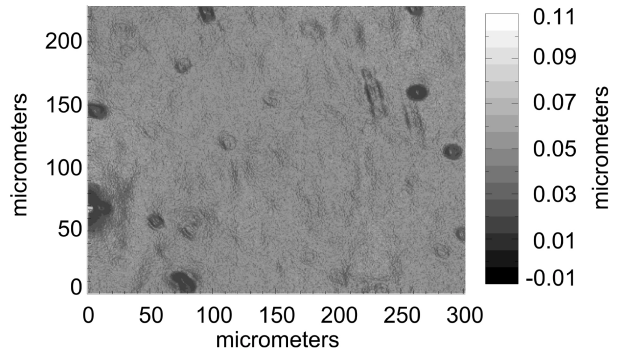

Figure 11. Typical surface topography map of the Sample C as measured by PSI Microscope of type 1; rms roughness = 5.0 nm.

C. Light Scattering Calculations

Calculations and measurements were performed for a number of angles but not all results are shown. The results for different angles of incidence are similar in nature.

In Fig. 12, (a) - (c), the relative reflectances measured and computed using the phase integral model and the different topography data are compared for incidence angles of 20° for the three samples. The same vertical logarithmic scale for all the graphs was used and the lower end of the y-scale was arbitrarily limited to 1×10^{-6}. The agreement between the measured and computed intensity distributions is good, especially if one takes into account that the logarithmic scale exaggerates the differences for angles that are further away from the specular direction. The broadening of the measured scattering distribution with increasing roughness is clearly reproduced by the computed distribution. The computed relative reflectance of Sample C differs little from that of a perfectly flat surface.

Figure 12. Comparison between relative reflectance curves as a function of scattering angle, measured and computed using a Schwartz window in the phase integral calculation.

The effect of the windowing function is shown in Fig. 13. For the roughest sample, Sample A, the windowing effect is small, as seen in Fig. 13 (a). For the smoother samples, B and C, different types of windows give varying intensities at angles away from the specular direction as shown in Fig. 13, (b) and (c).